Carbon Nanofibers Hot Paper

DOI: 10.1002/ange.201407103

Carbon Nanofibers Decorated with Molybdenum Disulfide Nanosheets: Synergistic Lithium Storage and Enhanced Electrochemical Performance**

*Fei Zhou, Sen Xin, Hai-Wei Liang, Lu-Ting Song, and Shu-Hong Yu**

Abstract: *Traditional lithium-ion batteries that are based on layered Li intercalation electrode materials are limited by the intrinsically low theoretical capacities of both electrodes and cannot meet the increasing demand for energy. A facile route for the synthesis of a new type of composite nanofibers, namely carbon nanofibers decorated with molybdenum disulfide sheets (CNFs@MoS_2), is now reported. A synergistic effect was observed for the two-component anode, triggering new electrochemical processes for lithium storage, with a persistent oxidation from Mo (or MoS_2) to MoS_3 in the repeated charge processes, leading to an ascending capacity upon cycling. The composite exhibits unprecedented electrochemical behavior with high specific capacity, good cycling stability, and superior high-rate capability, suggesting its potential application in high-energy lithium-ion batteries.*

Owing to significant advantages in terms of energy density and environmental sustainability, lithium-ion batteries (LIBs) have quickly dominated the consumer electronics market since the 1990s.[1] With their applications extending into large-scale energy storage fields, such as transportation and power grids, traditional LIBs that are based on layered Li intercalation electrode materials are limited by the intrinsically low theoretical capacities of both electrodes and cannot fulfill the increasing demand for energy density.[2] Against this background, anode materials that are based on novel Li storage mechanisms, such as conversion storage and interfacial storage, are especially promising owing to their predominant merits in capacity.[3] For example, molybdenum disulfide (MoS_2), a research hotspot for fuel cells and solar cells, has also been found to be a promising material for LIBs because of its two-dimensional layered morphology and the ability to host multiple Li ions, enabling its assembly with various substrates (e.g., graphene) and delivering a high theoretical specific capacity of 670 mA h g^{-1}.[4] Benefiting from their large specific surface areas and porous architectures, pyrolytic nanocarbon materials derived from carbohydrates feature numerous active sites for interfacial Li storage, so that they have high capacities that are several times larger than that of graphite.[5]

However, the use of these materials still involves many problems. MoS_2 is known to have a layered structure formed by tightly packed S–Mo–S motifs, which enables stable Li insertion above 1.1 V (vs. Li^+/Li, the same below), but it is converted into Mo and Li_2S upon further Li intercalation.[6] Once Li_2S is formed, it becomes the active component, and its electrochemistry dominates in the subsequent cycles.[4a] Owing to the low conductivity and poor cyclability of Li_2S, the capacity of MoS_2 often fades quickly upon cycling.[7] Meanwhile, as a conversion material, MoS_2 usually experiences a significant volume change during discharge/charge, leading to pulverization and resulting in poor cycling performance.[4c] On the other hand, an excessive interface between porous carbon and electrolyte leads to considerable side reactions, forming a thick solid electrolyte interface (SEI) on carbon and resulting in poor cyclability and a low Coulombic efficiency (CE) of $< 50\,\%$.[8] However, considering the complementary properties of the two components in terms of energy storage, a synergistic effect may be expected on their combination. Previous studies have shown that combining graphitized carbon materials (e.g., carbon nanotubes) with Li intercalation anode materials such as TiO_2 led to a synergistic effect, triggering enhanced kinetics and sometimes a novel mechanism for Li storage.[9] As a result, the composite exhibits a better electrochemical performance than either of the single components on their own.

Based on this concept, we herein report the synthesis of a novel nanocomposite, in which carbon nanofibers are decorated with MoS_2 sheets (CNFs@MoS_2) by a facile hydrothermal route with low-cost, biomass-derived carbonaceous nanofibers as the support. In serving as an anode material for LIBs, the CNF core acts as a host for Li storage, while also providing an efficient electron pathway for the fast lithiation/delithiation of MoS_2.[9] Meanwhile, the MoS_2 sheath helps to reduce the excessive surface area of the CNFs and promotes a rapid charge-transfer reaction by facilitating Li^+ migration. The cooperation of the two active components in

[*] F. Zhou,[+] Dr. S. Xin,[+] Dr. H. W. Liang, L. T. Song, Prof. Dr. S. H. Yu
Division of Nanomaterials and Chemistry, Hefei National Laboratory for Physical Sciences at Microscale, Collaborative Innovation Center of Suzhou Nano Science and Technology, Department of Chemistry, University of Science and Technology of China
Hefei 230026 (P. R. China)
E-mail: shyu@ustc.edu.cn
Homepage: http://staff.ustc.edu.cn/~yulab/
Dr. S. Xin[+]
Anhui Key Laboratory of Controllable Chemical Reaction and Material Chemical Engineering, School of Chemical Engineering
Hefei University of Technology
Hefei, Anhui 230009 (P. R. China)

[+] These authors contributed equally to this work.

[**] This work is supported by the National Basic Research Program of China (2010CB934700, 2013CB933900, 2014CB931800), the National Natural Science Foundation of China (21431006, 91022032, 91227103), the Chinese Academy of Sciences (KJZD-EW-M01-1), and the China Postdoctoral Science Foundation (2012M510160).

Supporting information for this article is available on the WWW under http://dx.doi.org/10.1002/anie.201407103.

 © 2014 Wiley-VCH Verlag GmbH & Co. KGaA, Weinheim

CNFs@MoS_2 brings about a favorable synergistic effect, leading to a higher capacity than that of the single components. Moreover, it also triggers new electrochemical processes for Li storage, by which a persistent transformation from Mo (or MoS_2) into MoS_3, which features larger capacity and better cyclability, is enabled during the repeated charge processes, resulting in a continuous increase in composite capacity upon cycling.

A double-coating approach was employed to synthesize CNFs@MoS_2, in which uniform hydrothermal carbonaceous nanofibers with an average diameter of 80 nm (Supporting Information, Figure S1 a, b) were used as supports, enabling the growth of MoS_2 nanosheets by a solution-based method.[10] The precursor was then annealed under nitrogen atmosphere to carbonize the core and crystallize the sheath, yielding the product (Scheme 1).

According to a scanning electron microscopy (SEM) image (Figure 1 a), CNFs@MoS_2 has a cable-like morphology with a uniform diameter distribution of 100–140 nm. The sheath consists of many curly nanosheets, as confirmed by a transmission electron microscopy (TEM) image (Figure 1 b). Different mass ratios of $(NH_4)_2MoS_4$ to CNFs ($R_{Mo/CNFs}$) were employed, among which only an optimal mass ratio $R_{Mo/CNFs} = 2.1$ yielded uniform nanofibers (Figure S2). A non-negligible interaction between oxygen-containing functional groups (OH, COOH) on carbonaceous nanofibers and Mo precursors in solution may explain the phenomenon.[11] A high-resolution TEM (HRTEM) image (Figure 1 c) demonstrates that the nanosheet consists of three to five layers, with an interlayer spacing of approximately 0.684 nm, close to the (002) spacing of hexagonal 2H-MoS_2 (0.621 nm). The X-ray diffraction (XRD) pattern (Figure S3 a) is indexed by a standard hexagonal 2H–MoS_2 structure (JPCDS 37-1492), yet with a blue shift in the (002) diffraction peak (from 16.71° to 14.08°), revealing an expanded interlayer. The expanded interlayer was once ascribed to the slow ramping rate upon annealing.[4c] However, considering the fast heating rate (5 °C min^{-1}) in this work, the expansion may not only be due to heating, but also due to the coaxial structure, which leads to an undulated surface and expansions. A HRTEM image of bare MoS_2 has clearly shown an unexpanded interlayer spacing of 0.632 nm (Figure S1 c, inset), further confirming our hypothesis. As the expanded interlayers are beneficial to Li intercalation upon initial discharge, a higher electroactivity of MoS_2 may be expected. An energy-dispersive X-ray (EDX) line-scan analysis along the cross section of the fiber reveals higher Mo and S contents at both sides and a higher C content at the center, indicating a co-axial structure (Figure 1 d). The result was further confirmed by elemental mapping (Figure 1 e–g), which revealed homogeneous sheath and core distributions of Mo/S and C, respectively. The CNFs@MoS_2 nanofibers contain approximately 72 wt % MoS_2, as determined by both thermogravimetric analysis (TGA, 71.89 wt %; Figure S3 b) and EDX analysis (72.23 wt %, Figure S4). The

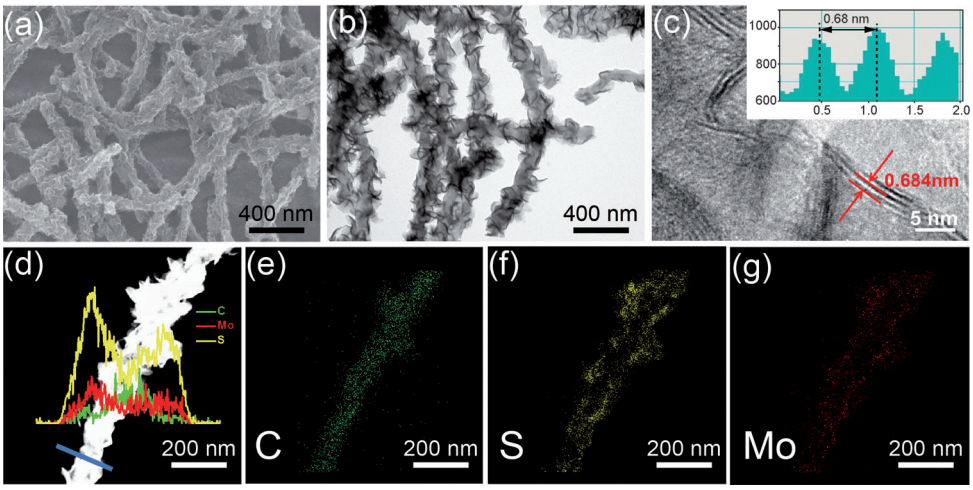

Figure 1. Structural characterization of CNFs@MoS_2: a) SEM image, b) TEM image, and c) HRTEM image. Inset: profile plot of the calibration for measuring the spacings. d) Annular dark-field STEM image. Inset: corresponding EDX line-scan profiles of C (green), Mo (red), and S (yellow) along the blue line. e–g) EDX elemental mappings of C, S, and Mo, respectively.

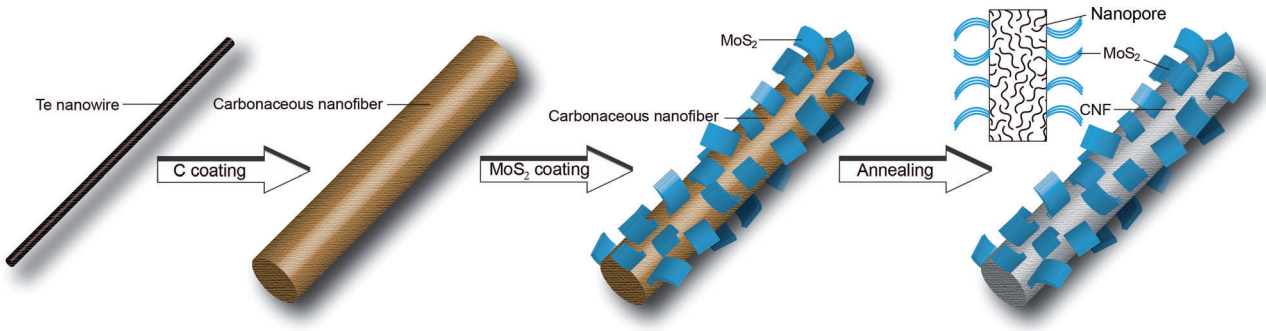

Scheme 1. Synthetic procedure for CNFs@MoS_2.

© 2014 Wiley-VCH Verlag GmbH & Co. KGaA, Weinheim

porous structure of CNFs@MoS_2 was further characterized by combined nitrogen adsorption/desorption isotherms (Figure S5a), with a large specific area of 176 $m^2 g^{-1}$ determined by the Brunauer–Emmett–Teller method, and a type I adsorption and a type H2 hysteresis loop separately indicating the existence of micropores and mesopores. The pore-size distribution calculated by density functional theory further revealed a hierarchically porous structure with micropores, mesopores, and macropores, which were due to the CNF core, the MoS_2 sheath, and the accumulated of fibers, respectively.[2a,9b]

The nanofibers were then assembled into Li half-cells to investigate their electrochemical performance. For comparison, bare CNFs and bare MoS_2 nanoparticles (Figure S1c,d) were also synthesized and tested. Figure 2a shows the galvanostatic discharge–charge (GDC) voltage profiles of CNFs@MoS_2 at 0.1 $A g^{-1}$. Upon the initial discharge, two plateaus appear at approximately 1.1 V and 0.6 V, corresponding to the phase transformation from 2H-MoS_2 to 1T Li_xMoS_2 and further decomposition into Li_2S and Mo nanoparticles, respectively.[4a,7] The sloped profile at >1.1 V corresponds to SEI formation on the surface of CNFs@MoS_2. Another sloped segment appearing at <0.5 V suggests interfacial Li uptake by the CNFs.[5a] The charge profile is also sloped, with a plateau at approximately 2.3 V, implying the oxidation of Li_2S.[2a,7b,12,13] The subsequent GDC cycles show sloped profiles, with two plateaus at approximately 1.85 V and 2.3 V upon discharge/charge, corresponding to electrochemical processes of Li_2S.[4a] In the first cycle, the discharge and charge capacities of CNFs@MoS_2 are 1489 and 983 mA h g^{-1}, respectively, which leads to a reasonable CE of 66% (Figure 2b). However, the bare CNFs show a much lower CE of 53.9% (Figure S6a). As the initial irreversible capacity loss is largely attributed to the formation of SEI, the CE improvement is largely due to the MoS_2 sheath, which helps to inhibit the side reactions of CNFs by diminishing their unfavorable contact with the electrolyte.

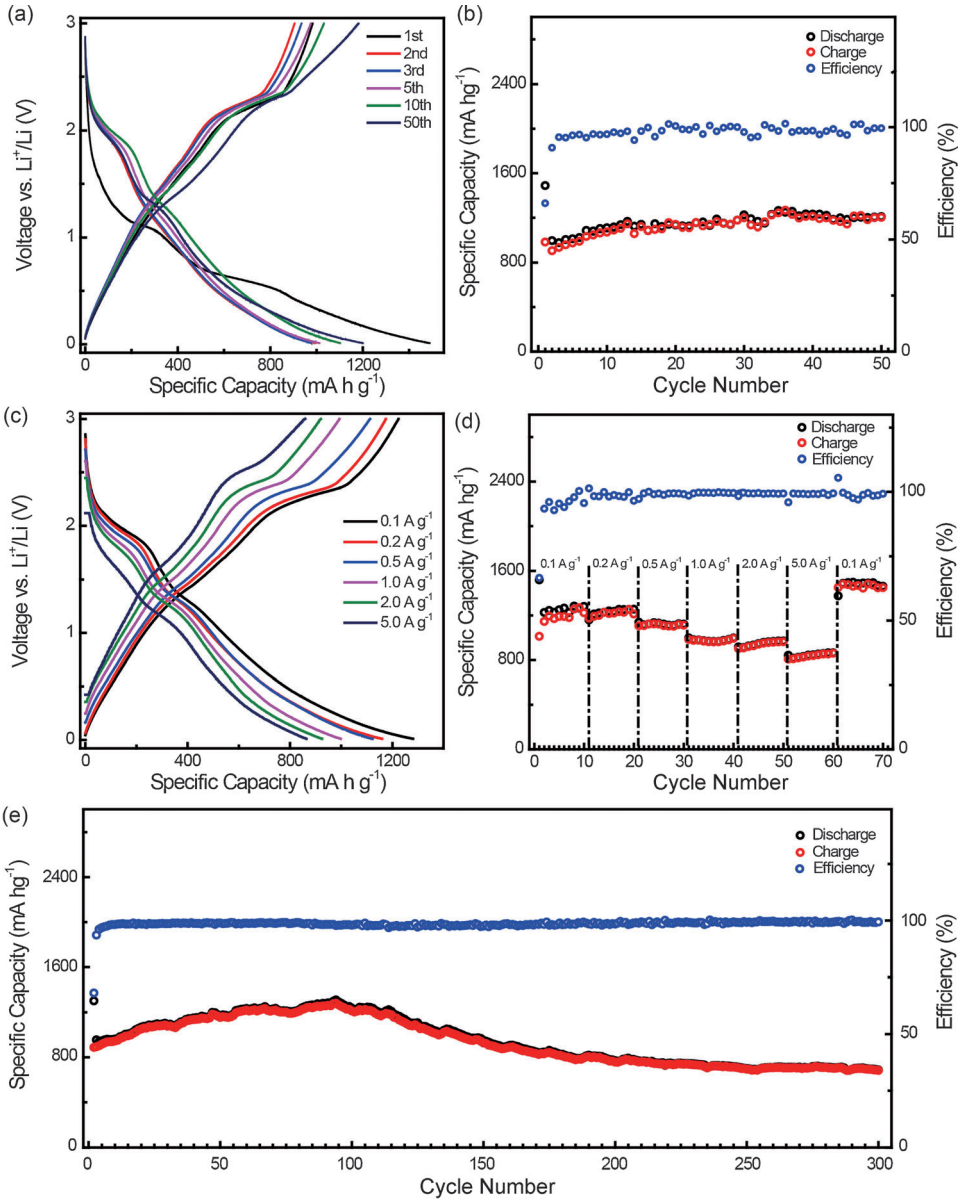

Figure 2. a) GDC profiles and b) cycling performance of CNFs@MoS_2 at 0.1 $A g^{-1}$. c) GDC profiles and d) cycling performance of CNFs@MoS_2 at different current densities. e) Long-life cycling performance of CNFs@MoS_2 at 1 $A g^{-1}$.

After several cycles, the CE quickly stabilizes at approximately 98%, further demonstrating the stabilizing effect of the MoS_2 sheath. After 50 cycles, the reversible capacity of CNFs@MoS_2 remains at 1264 mA h g^{-1} (Figure 2b), whereas bare CNFs and bare MoS_2 can only deliver 390 mA h g^{-1} and 124 mA h g^{-1}, respectively (Figure S6a,c). As the composite capacities significantly exceed those outputted by the individual components, a synergistic effect between the CNFs and MoS_2 is observed.

The CNFs@MoS_2 nanocomposite also exhibits improved cycling and rate performance. Even at 1 $A g^{-1}$, the CNFs@MoS_2 still demonstrates a high capacity of 688 mA h g^{-1} with a CE approaching 100% after 300 cycles, implying an excellent high-rate stability (Figure 2e). Upon gradually elevating the current density, the GDC profiles of

© 2014 Wiley-VCH Verlag GmbH & Co. KGaA, Weinheim

CNFs@MoS_2 remain stable (Figure 2c), and a high capacity of 864 mA h g^{-1} is retained at 5 A g^{-1} (Figure 2d). At the same current density, the bare CNFs and the bare MoS_2 can only deliver 60 mA h g^{-1} and 12 mA h g^{-1} (Figure S6b,d). After decreasing the current density back to 0.1 A g^{-1}, the capacity of CNFs@MoS_2 quickly increases to 1376 mA h g^{-1} (Figure 2d), disclosing a fine capacity recovery.

Moreover, the capacity of CNFs@MoS_2 shows an unusual ascending trend at various current densities during the initial tens of cycles (Figure 2b,d,e). To reveal the electrochemistry behind this trend, cyclic voltammograms (CVs) of CNFs@MoS_2 and bare MoS_2 were collected at a slow scan rate (0.05 mV s^{-1}). In the first cathodic process, two reduction peaks appear at approximately 0.95 V and 0.41 V (Figure 3a), corresponding well with Li intercalation into layered MoS_2 and conversion into Mo and Li_2S. In the first anodic process, however, three oxidation peaks appear, with two small peaks at approximately 1.47 V and 1.74 V. As the potential difference between the two peaks corresponds to the difference between the standard electrode potentials of MoO_2/Mo (−0.15 V) and H_2MoO_4/Mo (0.11 V; both under acidic conditions), the two peaks may be associated with the stepped oxidations from Mo to Mo^{4+} and to Mo^{6+}, respectively. Another oxidation peak at approximately 2.39 V is due to the oxidation of Li_2S. The initial cathodic CV of bare MoS_2 also featured the Li intercalation (1.03 V) and the conversion reaction (0.50 V), yet no peak corresponding to the oxidation from Mo to Mo^{6+} was observed in the anodic process (Figure S7). Therefore, it is clear that the CNFs do assist in Mo oxidation to Mo^{6+} during charging. In the subsequent CNFs@MoS_2 CVs, the profiles become highly consistent, and three distinct pairs of redox peaks appear: Two reduction peaks at approximately 1.55 V and 1.24 V separately correspond to the oxidation peaks at about 1.47 V and 1.74 V, and together they denote the stepped reductions/oxidations between Mo^{6+} and Mo. The reduction peak at approximately 1.85 V corresponds to the oxidation peak at about 2.38 V, denoting the sulfide redox reaction.[4a,7] The peaks at approximately 0.95 V and 0.41 V significantly weakened and became hardly differentiable after five CV scans, implying the depletion of 2H-MoS_2. The sloped profile at < 0.3 V was also observed in repeated cathodic processes, confirming reversible Li uptake/release of the CNFs.[5a]

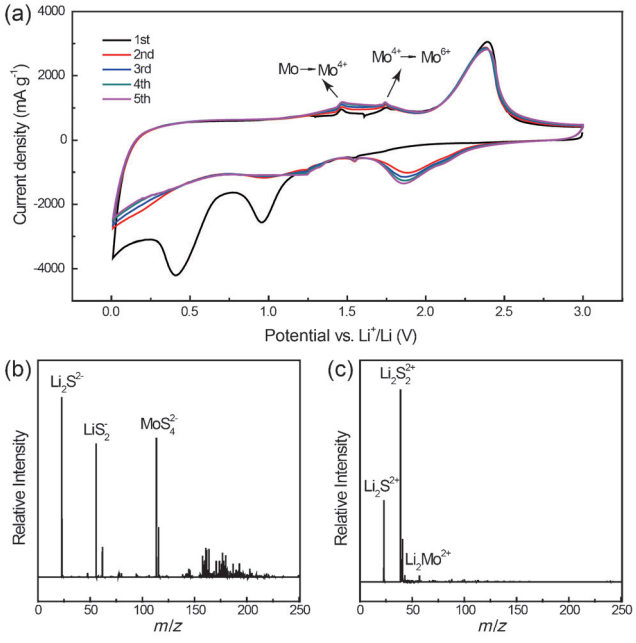

Figure 3. a) The first five CVs of the CNFs@MoS_2 anode. b,c) Mass spectra of the sample before (b) and after (c) the initial charge process (CNFs@MoS_2-1).

To confirm the nature of the above-described electrochemical process of molybdenum sulfides, ex situ techniques, including TEM, X-ray photoelectron spectroscopy (XPS), and mass spectrometry (MS), were employed to characterize a CNFs@MoS_2 anode before use, in its fully discharged state, and in its fully charged state, respectively. For pristine CNFs@MoS_2, the binding energies of Mo $3d_{3/2}$ and Mo $3d_{5/2}$ are 233.0 and 229.8 eV, respectively (Figure S8a), indicating the existence of Mo^{4+}. At the fully discharged state, Mo nanoparticles were clearly distinguishable from the fiber surface (Figure S9a). After the initial charge process (denoted as CNFs@MoS_2-1), MoS_4^{2-} fragments (Figure 3b) and Li_2Mo^{2+} fragments (Figure 3c) were observed in the MS spectra, separately indicating the existence of MoS_3 and Mo. After the tenth charge cycle (denoted as CNFs@MoS_2-10), the Mo binding energies shifted to 235.6 and 232.4 eV, confirming the generation of Mo ions with a higher valance (i.e., Mo^{6+}, see Figure S8b).

Therefore, the electrochemical processes of Mo have been clarified: The initial cathodic process involves the lithiation of MoS_2 to form Mo and Li_2S, yet the reverse anodic process leads to the generation of Mo^{6+} sulfides (mostly MoS_3), with a certain amount of unoxidized Mo remaining. The lithiation/delithiation of MoS_3 becomes highly reversible from the second scan, and the oxidation from Mo to Mo^{6+} proceeds in the subsequent scans, consuming the unoxidized Mo (also the unreacted 2H-MoS_2) and generating more MoS_3. This point is corroborated by the gradually enhanced redox peaks of Mo^{6+} upon scanning (Figure 3a). With the depletion of MoS_2, MoS_3 gradually becomes a major active component of the composite, and its electrochemistry, together with the Li_2S electrochemistry, dominates subsequently.

Herein, a synergistic effect between the CNFs and MoS_2 may account for the unique electrochemistry of CNFs@MoS_2. Owing to their high electronic conductivity, CNFs act both as a Li storage matrix and as a conductive support for MoS_2, providing sufficient e^- for lithiation/delithiation of the sheath. Upon discharging, Mo nanoparticles uniformly embed in Li_2S (Figure S9a) to cover the conductive CNFs. With close contacts between Li_2S, Mo, and CNF, the outward transmission of e^- is prompted in the Li release process, leading to the generation of Mo^{6+} upon charging. Commonly, Li_2S generated during the initial discharge process has a low electroactivity and cannot be fully oxidized to S (but to soluble polysulfides) upon charging, which may deteriorate the capacity and cyclability of MoS_2. The conductive CNFs enhance the electroactivity of Li_2S by facilitating its delithiation process, while the in situ generated Mo^{6+}, with its higher affinity for sulfur-containing molecules than Mo^{4+}, binds surrounding polysulfides (on or near the surface of the Mo

 © 2014 Wiley-VCH Verlag GmbH & Co. KGaA, Weinheim

nanoparticles) to form MoS_3, thus preventing the irreversible loss of active S.[4a,7a,14] With the transformation of electrochemically inactive and unstable Li_2S into active and stable MoS_3 upon charging, the hybrid anode exhibits a much more stabilized electrochemistry than bare MoS_2 (Figure S7), while also featuring ascending S utilization, which explains the increase in capacity during the initial tens of cycles. Electrochemical-impedance-spectroscopy results show that compared to pristine CNFs@MoS_2, CNFs@MoS_2-1 and CNFs@MoS_2-10 exhibit significantly reduced charge-transfer resistances (Figure S10). Therefore, the kinetic performance of the composite material is improved upon cycling, which is consistent with the above electroactive process of CNFs@MoS_2.

Finally, the synergistic effect and the structural advantages of CNFs@MoS_2 also contribute to its excellent performance in long-life cycling and high-rate tests. Whereas the CNF core enables fast e^- transmission for the MoS_2 sheath, the mesoporous MoS_2 sheath provides an unperturbed Li^+ supply for the CNF core, improving the Li storage kinetics and the stability of both components. Meanwhile, the rigid structure of the CNFs effectively relieves the volume change of MoS_2 upon lithiation/delithiation, and helps in the formation of a hierarchically conductive network with carbon black on a micrometer scale, thus improving the cycling stability and high-rate capability. It was observed for a cycled anode that CNFs@MoS_2 still kept its original cable structure (Figure S9b and Figure S11a), with uniformly distributed C, Mo, and S along the cable (Figure S11b–d), demonstrating the fine cycling stability of the composite.

In summary, we have successfully developed a simple strategy to synthesize well-defined CNFs@MoS_2 coaxial nanofibers. When they are used as anode materials for LIBs, the cooperation of the two active components in CNFs@MoS_2 leads to a synergistic effect, triggering new electrochemical processes for the Li storage of MoS_2, through which electrochemically active and stable MoS_3 persistently forms in the charge process, leading to an increased capacity upon cycling. The synergistic effect also helps to build a hierarchically conductive network, contributing to much improved electrode kinetics and cycling stability. The CNFs@MoS_2 nanofibers exhibit excellent Li storage properties in terms of specific capacity (1489 $mA\,h\,g^{-1}$ upon initial discharge), cycling performance (1264 $mA\,h\,g^{-1}$ after 50 cycles) and rate performance (860 $mA\,h\,g^{-1}$ at 5 $A\,g^{-1}$), making it a promising anode material for high-energy LIBs. Moreover, in the light of the notable capacity advantages of non-intercalation materials in high-energy batteries, the present findings on the synergistic effect in CNFs@MoS_2 are expected to have far-reaching significance over previous works on intercalation materials,[9b] and make this strategy simple yet inspiring. Furthermore, this work could provide insights that enable further improvements of the performance of lithium–sulfur batteries.

Received: July 10, 2014
Published online: September 11, 2014

Keywords: carbon nanofibers · electrochemistry · lithium-ion battery · molybdenum · nanostructures

[1] a) M. Armand, J. M. Tarascon, *Nature* **2008**, *451*, 652–657; b) L. X. Yuan, Z. H. Wang, W. X. Zhang, X. L. Hu, J. T. Chen, Y. H. Huang, J. B. Goodenough, *Energy Environ. Sci.* **2011**, *4*, 269–284; c) Y. Chen, S. A. Freunberger, Z. Peng, F. Bardé, P. G. Bruce, *J. Am. Chem. Soc.* **2012**, *134*, 7952–7957; d) M. J. Armstrong, C. O'Dwyer, W. J. Macklin, J. D. Holmes, *Nano Res.* **2014**, *7*, 1–62.

[2] a) Y. X. Yin, S. Xin, Y. G. Guo, L. J. Wan, *Angew. Chem. Int. Ed.* **2013**, *52*, 13186–13200; *Angew. Chem.* **2013**, *125*, 13426–13441; b) S. Xin, L. Gu, N. H. Zhao, Y. X. Yin, L. J. Zhou, Y. G. Guo, L. J. Wan, *J. Am. Chem. Soc.* **2012**, *134*, 18510–18513; c) H. Sun, G. L. Xu, Y. F. Xu, S. G. Sun, X. Zhang, Y. Qiu, S. Yang, *Nano Res.* **2012**, *5*, 726–738; d) H. Fei, Z. Peng, L. Li, Y. Yang, W. Lu, E. G. Samuel, X. Fan, J. Tour, *Nano Res.* **2014**, *7*, 1–9.

[3] a) Y. Kim, Y. Park, A. Choi, N. S. Choi, J. Kim, J. Lee, J. H. Ryu, S. M. Oh, K. T. Lee, *Adv. Mater.* **2013**, *25*, 3045–3049; b) L. Qie, W. M. Chen, Z. H. Wang, Q. G. Shao, X. Li, L. X. Yuan, X. L. Hu, W. X. Zhang, Y. H. Huang, *Adv. Mater.* **2012**, *24*, 2047–2050.

[4] a) T. Stephenson, Z. Li, B. Olsen, D. Mitlin, *Energy Environ. Sci.* **2014**, *7*, 209–231; b) Y. Shi, Y. Wang, J. I. Wong, A. Y. S. Tan, C. L. Hsu, L. J. Li, Y. C. Lu, H. Y. Yang, *Sci. Rep.* **2013**, *3*, 2169; c) H. Liu, D. Su, R. Zhou, B. Sun, G. Wang, S. Z. Qiao, *Adv. Energy Mater.* **2012**, *2*, 970–975; d) X. Cao, Y. Shi, W. Shi, X. Rui, Q. Yan, J. Kong, H. Zhang, *Small* **2013**, *9*, 3433–3438.

[5] a) J. R. Dahn, T. Zheng, Y. Liu, J. S. Xue, *Science* **1995**, *270*, 590–593; b) T. Zheng, Y. Liu, E. W. Fuller, S. Tseng, U. von Sacken, J. R. Dahn, *J. Electrochem. Soc.* **1995**, *142*, 2581–2590; c) H. Li, Z. Wang, L. Chen, X. Huang, *Adv. Mater.* **2009**, *21*, 4593–4607.

[6] a) X. Huang, Z. Zeng, H. Zhang, *Chem. Soc. Rev.* **2013**, *42*, 1934–1946; b) X. Huang, C. Tan, Z. Yin, H. Zhang, *Adv. Mater.* **2014**, *26*, 2185–2204; c) H. Li, J. Wu, Z. Yin, H. Zhang, *Acc. Chem. Res.* **2014**, *47*, 1067–1075; d) Y. Huang, J. Wu, X. Xu, Y. Ho, G. Ni, Q. Zou, G. Koon, W. Zhao, A. H. Castro Neto, G. Eda, C. Shen, B. Özyilmaz, *Nano Res.* **2013**, *6*, 200–207.

[7] a) K. Chang, W. Chen, *ACS Nano* **2011**, *5*, 4720–4728; b) L. Yang, S. Wang, J. Mao, J. Deng, Q. Gao, Y. Tang, O. G. Schmidt, *Adv. Mater.* **2013**, *25*, 1180–1184.

[8] Y. Yan, Y. X. Yin, S. Xin, Y. G. Guo, L. J. Wan, *Chem. Commun.* **2012**, *48*, 10663–10665.

[9] a) S. Xin, Y. G. Guo, L. J. Wan, *Acc. Chem. Res.* **2012**, *45*, 1759–1769; b) F. F. Cao, Y. G. Guo, S. F. Zheng, X. L. Wu, L. Y. Jiang, R. R. Bi, L. J. Wan, J. Maier, *Chem. Mater.* **2010**, *22*, 1908–1914.

[10] a) H. W. Liang, J. W. Liu, H. S. Qian, S. H. Yu, *Acc. Chem. Res.* **2013**, *46*, 1450–1461; b) H. W. Liang, W. J. Zhang, Y. N. Ma, X. Cao, Q. F. Guan, W. P. Xu, S. H. Yu, *ACS Nano* **2011**, *5*, 8148–8161; c) H. W. Liang, Q. F. Guan, L. F. Chen, Z. Zhu, W. J. Zhang, S. H. Yu, *Angew. Chem. Int. Ed.* **2012**, *51*, 5101–5105; *Angew. Chem.* **2012**, *124*, 5191–5195.

[11] Y. G. Li, H. L. Wang, L. Xie, Y. Y. Liang, G. S. Hong, H. J. Dai, *J. Am. Chem. Soc.* **2011**, *133*, 7296–7299.

[12] X. P. Fang, C. X. Hua, X. W. Guo, Y. S. Hu, Z. X. Wang, X. P. Gao, F. Wu, J. Z. Wang, L. Q. Chen, *Electrochim. Acta* **2012**, *81*, 155–160.

[13] a) J. Xiao, X. Wang, X. Q. Yang, S. Xun, G. Liu, P. K. Koech, J. Liu, J. P. Lemmon, *Adv. Funct. Mater.* **2011**, *21*, 2840–2846; b) X. Fang, X. Guo, Y. Mao, C. Hua, L. Shen, Y. Hu, Z. Wang, F. Wu, L. Chen, *Asian J. Chem.* **2012**, *24*, 1013–1017.

[14] a) L. Wang, Z. Xu, W. Wang, X. Bai, *J. Am. Chem. Soc.* **2014**, *136*, 6693–6697; b) Y. Yang, M. T. McDowell, A. Jackson, J. J. Cha, S. S. Hong, Y. Cui, *Nano Lett.* **2010**, *10*, 1486–1491.

 © 2014 Wiley-VCH Verlag GmbH & Co. KGaA, Weinheim